Journal of Power Sources 196 (2011) 2819–2825

Contents lists available at ScienceDirect

Journal of Power Sources

journal homepage: www.elsevier.com/locate/jpowsour

The electrochemical behaviour of the carbon-coated $Ni_{0.5}TiOPO_4$ electrode material

Kenza Maher [a], Kristina Edström [b], Ismael Saadoune [a,*], Torbjörn Gustafsson [b], Mohammed Mansori [a]

[a] ECME, FST Marrakech, University Cadi Ayyad, BP549, Av. A. Khattabi, Marrakech, Morocco
[b] Department of Materials Chemistry, Uppsala University, Box 538, SE-751 21 Uppsala, Sweden

ARTICLE INFO

Article history:
Received 25 August 2010
Received in revised form 13 October 2010
Accepted 7 November 2010
Available online 12 November 2010

Keywords:
$Ni_{0.5}TiOPO_4$
Lithium ion batteries
Carbon coating
Synchroton diffraction

ABSTRACT

$Ni_{0.5}TiOPO_4$ oxyphosphate exhibits good electrochemical properties as an anode material in lithium ion batteries but suffers from its low conductivity. We present here the electrochemical performances of the synthesized $Ni_{0.5}TiOPO_4$/carbon composite by using sucrose as the carbon source. X-ray diffraction study confirms that this phosphate crystallizes in the monoclinic system (S.G. $P2_1/c$). The use of the $Ni_{0.5}TiOPO_4$/C composite in lithium batteries shows enhanced electrochemical performances compared with the uncoated material. Capacities up to 200 mAh g^{-1} could be reached during cycling of this electrode. Furthermore, an acceptable rate capability was obtained with very low capacity fading even at 0.5C rate. Nevertheless, a considerable irreversible capacity was evidenced during the first discharge. *In situ* synchrotron X-ray radiation was utilized to study the structural change during the first discharge in order to evidence the origin of this irreversible capacity. Lithium insertion during the first discharge induces an amorphization of the crystal structure of the parent material accompanied by an irreversible formation of a new phase.

1. Introduction

Lithium-ion batteries (Li-ion) are interesting devices for electrochemical energy storage for most emerging green technologies such as wind and solar technologies or hybrid and plug-in electric vehicles. Compared with conventional aqueous rechargeable cells, such as nickel–cadmium and nickel–metal hydrid, Li-ion cells have higher energy densities, higher operating voltages, lower self-discharge and lower maintenance requirements [1]. Present commercial lithium-ion batteries use $LiCoO_2$ or $LiMn_2O_4$ as cathode materials, and graphite or carbonaceous materials as anode materials [2].

In many cases, the anode material can play the key role on the safety of the battery. Anode materials continue to attract attention with the aim of developing a material able to accommodate lithium reversibly with a higher capacity than carbon. Thus, many materials were proposed as anode materials for lithium-ion batteries to replace graphite or carbonaceous materials such as, composite alloys [3,4], tin oxides [5–8], transition metal oxides [9–11], vanadates [12] and spinel lithium titanates $Li_4Ti_5O_{12}$ [13].

Recently Belharouak and Amine [14] proposed $Ni_{0.5}TiOPO_4$ titanium oxyphosphate as new lithium insertion material for Li-ion batteries. A first testing of $Ni_{0.5}TiOPO_4$ has shown an irreversible capacity of 415 mAh g^{-1}, corresponding to the insertion of three lithium ions, at a current density of 0.1 mA cm^{-2}, between 0.5 and 4 V. Nevertheless, a notable capacity fade was observed after a few cycles. We recently reported the electrochemical behaviour of $Li_{0.5}Ni_{0.25}TiOPO_4$ homologous material and showed that their cycling performances were notably improved by carbon coating [15]. Indeed, both of these oxyphosphates exhibit electrochemical features evidencing that they are candidates for the negative electrode of the lithium ion batteries.

In fact, titanium oxyphosphate $Ni_{0.5}TiOPO_4$ was firstly reported by Gravereau et al. [16]. $Ni_{0.5}TiOPO_4$ crystallizes in the monoclinic system with $P2_1/c$ space group. The 3-dimensional framework is built up from [TiO_6] octahedra and [PO_4] tetrahedra. [TiO_6] octahedra are linked together by corners and form infinite chains along the *c*-axis (Fig. 1). These chains are linked together by [PO_4] tetrahedra. Nickel atoms are located in an octahedral sites (2a site) sharing two faces with two [TiO_6] octahedra. The material also contains octahedral vacant sites that constitute favourable way for lithium insertion. However, as many of phosphates, $Ni_{0.5}TiOPO_4$ exhibits a low electronic conductivity reducing notably its electrochemical performances.

In this paper, we report the synthesis of $Ni_{0.5}TiOPO_4$/C composite using sucrose as the carbon source. The obtained composite was characterized by X-ray diffraction (XRD) and thermogravimetry (TG). The electrochemical properties of these composites were

* Corresponding author. Tel.: +212 6 61 48 64 64; fax: +212 5 24 43 31 70.
E-mail address: saadoune1@yahoo.fr (I. Saadoune).

0378-7753/$ – see front matter © 2010 Elsevier B.V. All rights reserved.
doi:10.1016/j.jpowsour.2010.11.044

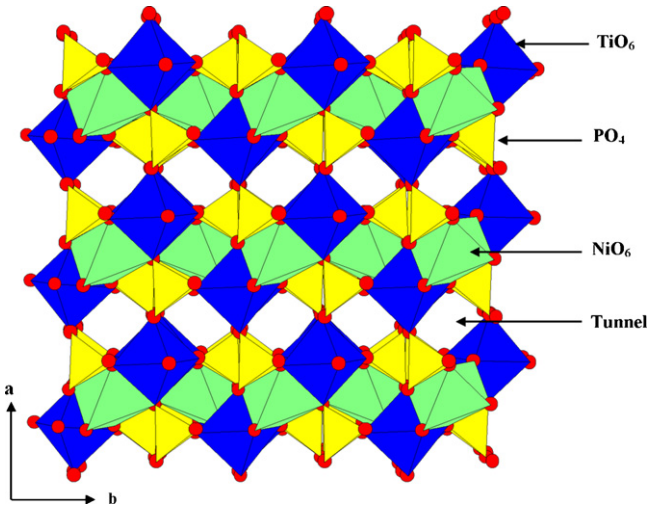

Fig. 1. Structure of $Ni_{0.5}TiOPO_4$.

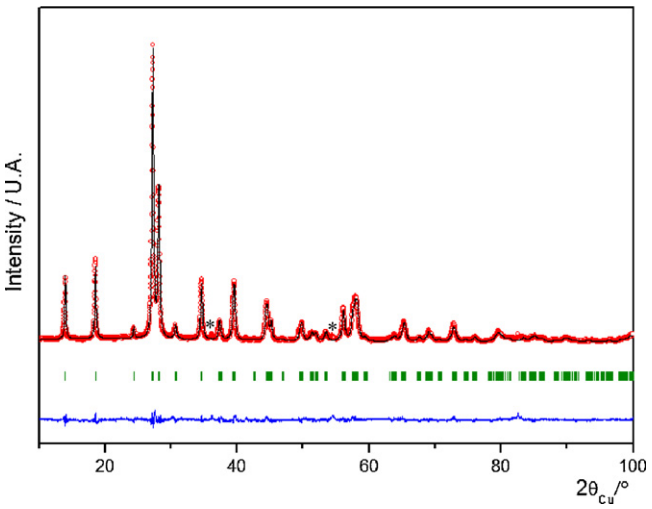

Fig. 2. X-ray powder diffractogram of $Ni_{0.5}TiOPO_4$/C. TiO_2 peaks are marked with asterisks (*).

investigated by the galvanostatic charge/discharge method and cyclic voltammetry.

In order to understand the relationship between the electrochemical performance and the structure changes involved in $Li_xNi_{0.5}TiOPO_4$ during lithium insertion/extraction, *in situ* XRD using synchrotron X-ray source was performed.

2. Experimental

The $Ni_{0.5}TiOPO_4$/C was prepared from a stoichiometric mixture of an aqueous solution of $Ni(NO_3)_2{\cdot}6H_2O$ (99%, Aldrich), and $(NH_4)_2HPO_4$ (98%, Merck) with a solution of $TiCl_4$ (99%, Aldrich) diluted in ethanol. After evaporation at 45 °C under vacuum, the resulting powder was heated up to 400 °C for 5 h to remove ammonia and water. Finally, the powder was fired up to 900 °C for 12 h. The resulting powder was mixed and rigorously stirred with 10% in mass of sucrose in acetone. After evaporation of the acetone, the mixture was heated at 300 °C for 6 h in Ar atmosphere.

Powder X-ray diffraction (XRD) patterns were collected with a Siemens D5000 diffractometer in reflection mode using CuK_α radiation. XRD patterns were collected between 10° and 100° with 0.02° step size and 30 s counting time, and were refined by the Rietveld method using the Fullprof software [17].

The carbon content was estimated from the thermogravimetric analysis (TGA). TG data were recorded using TGA Q500 instrument under a purified air flow from 100 °C to 800 °C at a heating rate of 10 °C min^{-1}.

Electrochemical measurements were performed in lithium cells containing a lithium foil as negative electrode. Positive electrodes were prepared by spreading a mixture of 75% active material, 10% super-P carbon powder, and 15% of PVDF [poly(vinylidene fluoride)] in NMP (1-methyl-2pyrrolidinone) onto an aluminium foil. The coated aluminium was transferred into an argon-filled glove box (<1 ppm H_2O and O_2) and dried under vacuum at 120 °C overnight. The cathode, a Celgard separator soaked in an electrolyte and the anode were assembled in a "coffee-bag" [18] (polymer laminated aluminium foil) type cell. The electrolyte was 1 M $LiPF_6$ (lithium hexafluorophosphate) dissolved in a 2:1 volume ratio solution of EC (ethylene carbonate) and DEC (diethyl carbonate). Cyclic voltammetry was performed between 0.9 and 3.0 V at a scan rate 0.01 mV s^{-1}. Discharge–charge cycle test was carried out between 0.9 and 3.0 V vs. Li^+/Li with different rates.

In situ synchrotron diffraction was collected on beamline I911-5 at MAX-lab (National Laboratory for Synchrotron Radiation, Sweden) using a Mar 165 detector. The monochromator (λ = 0.91 Å) was equipped with a bent Si (2 2 0) crystal.

For the *in situ* study, the mass of the electrodes was around 20 mg. The cell was first discharged to 0.9 V, then charged to 3 V and discharged again with the same current rate of C/5.

3. Results and discussion

3.1. X-ray diffraction

Fig. 2 shows the XRD patterns of the $Ni_{0.5}TiOPO_4$/C composite obtained by co-precipitation method. The XRD refinement was carried out in the monoclinic system with $P2_1/c$ space group. The diffraction peaks indicate a high degree of crystallinity of the material, with two very weak peaks labelled by asterisk (*) corresponding to less than 2% of TiO_2 impurity which could be neglected in the following characterizations. The main parameters deduced from the refinements of the XRD data and the cationic distributions determined for the material are summarized in Table 1. The reliability factors (R_F = 0.02, R_B = 0.024, R_p = 0.072, R_{wp} = 0.10 and χ^2 = 2.17) are in good agreement with those published by Gravereau et al. [16]. It should be noticed that no traces of carbon have been detected in the XRD pattern of the studied compound indicating that the residual carbon is in an amorphous state.

3.2. TG analysis

Fig. 3 shows the thermogravimetric curve of $Ni_{0.5}TiOPO_4$/C composite. The TGA clearly shows that the weight loss takes place in one step between 260 and 530 °C. The weight loss is about 3.7%. This weight loss was attributed to the departure of CO_2 gas as a result of the reaction of the residual carbon with the oxygen (air atmosphere). As demonstrated in our previous study [15], the residual carbon prevents the growth of $Ni_{0.5}TiOPO_4$ particles, which results in a small particles size. The presence of the carbon in the studied composite, even with low concentration, is expected to boost the electrochemical performances of $Ni_{0.5}TiOPO_4$.

3.3. Electrochemistry

Fig. 4 shows the cyclic voltammograms (CV) of the first two cycles of the Li//$Ni_{0.5}TiOPO_4$/C cell between 0.9 and 3 V. The interesting feature is the difference between the first and second discharges evidencing an important irreversible phenomenon accompanied the lithium insertion during the first cycle.

Table 1
Crystallographic parameters of $Ni_{0.5}TiOPO_4$/C deduced from the Rietveld refinement.

Crystal system: monoclinic; space group: $P2_1/c$ (a = 7.3829(3) Å; b = 7.3301(3) Å; c = 7.3499(3) Å; β = 120.23(2)°)						
Atom	Wyckoff site	x	y	z	Occupancy	B (Å)
Ni	2a	0.00000	0.00000	0.00000	1.00	1.02(7)
Ti	4e	0.7332(1)	0.2276(1)	0.5298(4)	1.00	0.64(1)
P	4e	0.2435(4)	0.1268(3)	0.7389(9)	1.00	0.68(4)
O(1)	4e	0.7755(8)	0.1510(3)	0.7819(9)	1.00	0.37(8)
O(2)	4e	0.80541(3)	0.0009(2)	0.1045(4)	1.00	0.37(8)
O(3)	4e	0.4380(1)	0.2417(6)	0.8944(1)	1.00	0.37(8)
O(4)	4e	0.2822(2)	0.0166(2)	0.5973(2)	1.00	0.37(8)
O(5)	4e	0.0557(1)	0.2388(8)	0.1438(4)	1.00	0.37(8)

Conditions of the run	
Temperature	300 K
Angular range	$10° \leq 2\theta \leq 100°$
Step scan increment (2θ)	0.02°
Zero point (2θ)	−0.03712
Number of fitted parameters	45
Profile parameters	$PV = \eta L + (1-\eta)G$
Half-width parameters	U = 0.2049 (8); V = −0.0214 (2); W = 0.0365 (2)
Reliability factors	R_F = 2.0%; R_B = 2.4%; R_p = 7.15%; R_{wp} = 9.9%; χ^2 = 2.17

The first cathodic scan shows two reduction peaks, at 1.2 V and 1.07 V. While the subsequent anodic scan shows two new peaks at 1.68 and 1.82 V but no evidence of signals in the 0.9–1.6 V potential range. For the second cycle, two cathodic peaks at about 1.77 V and 1.60 V and two anodic peaks observed at 1.7 and 1.83 V were registered showing a good reversibility of the electrochemical process in the studied material.

This irreversibility during the first discharge is related to a structural change, as discussed later. No further changes in the voltammogram were observed after the first cycle, suggesting that all major changes occurred in that first discharge.

Fig. 5 shows two first discharge/charge curves for Li//$Ni_{0.5}TiOPO_4$/C cell at C/20 rate. The initial open-circuit voltage (OCV) is 3.17 V. During the first discharge (Li insertion), the voltage drops quickly down to 1.14 V, followed by two adjacent weak plateaus at about 1.13 and 1 V, respectively. The existence of these two last plateaus is clearly confirmed by the variation of the incremental capacity with the potential plotted also in Fig. 5.

In the 1st plateau, the capacity potential region is equal to 147 mAh g^{-1} which corresponds to the intercalation of ~1 mol of lithium ion per formula unit. The capacity reaches approximately 350 mAh g^{-1} in the second plateau corresponding to 2.5 mol of Li per mol of $Ni_{0.5}TiOPO_4$. It should be noticed that all these plateaus are practically indistinguishable and seem to be overlapped. This probably means that only one structural/electronic phenomenon is involved during the first irreversible lithium insertion. Furthermore, it is well known that Ti^{4+}/Ti^{3+} couple is active around 1.5 V as observed in many electrode materials such as $Li_{0.5}Ni_{0.25}TiOPO_4$ [15] or $Li_4Ti_5O_{12}$ [19–21]. Nevertheless, the recorded potential plateaus during the first discharge of the Li//$Ni_{0.5}TiOPO_4$/C cell are less than 1.14 V. Thus, Ti^{4+} reduction during the first discharge is accompanied by an irreversible process inducing a high cell polarization.

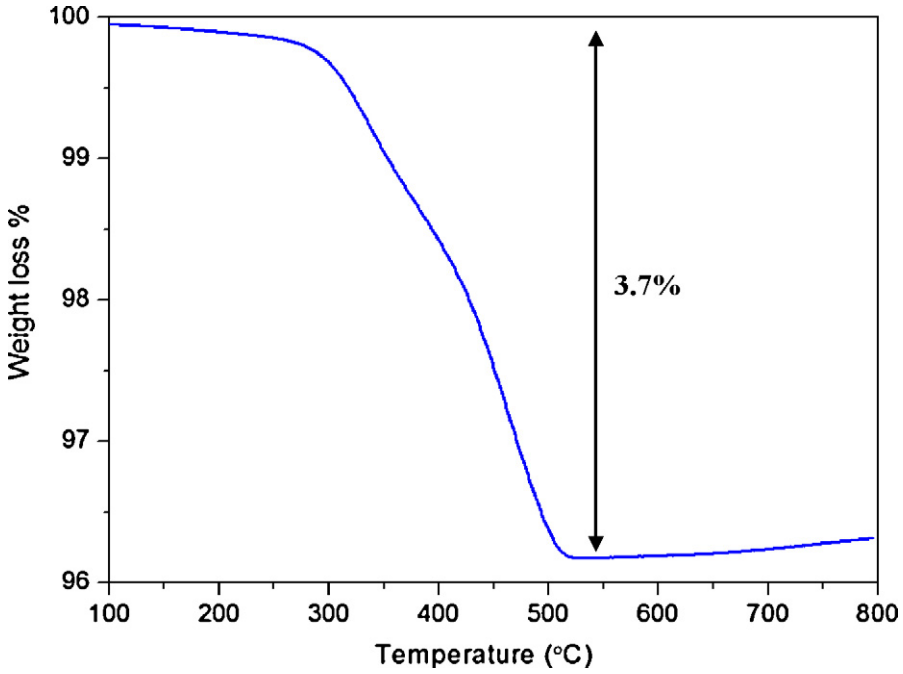

Fig. 3. TG curve of $Ni_{0.5}TiOPO_4$/C composite recorded in air atmosphere.

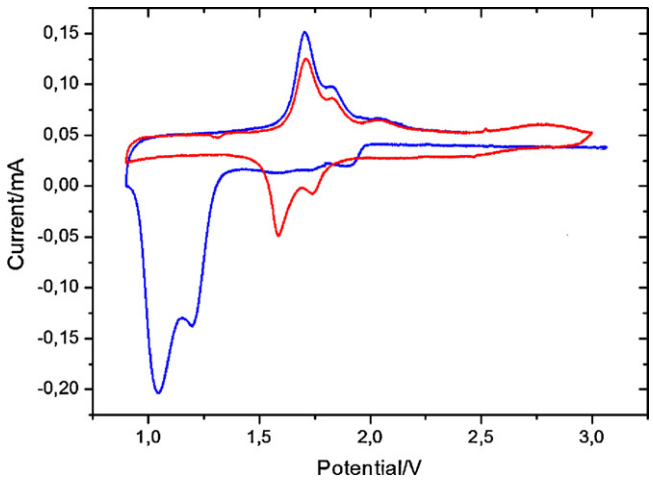

Fig. 4. CV plots of the Li//$Ni_{0.5}TiOPO_4$/C cell cycled between 0.9 and 3 V. Scan rate 0.01 mV s^{-1}.

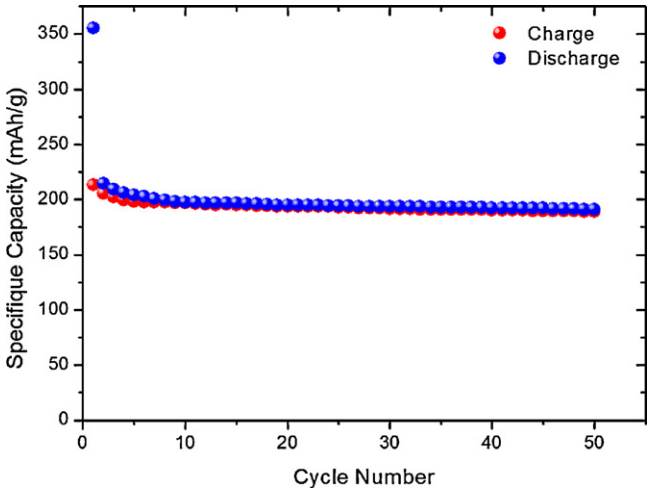

Fig. 6. Discharge–charge capacities for the Li//$Ni_{0.5}TiOPO_4$/C cell during 50 cycles at a C/20 rate in the 0.9–3 V potential range.

The first charge (Li extraction) profile shows a continuous increase of the voltage up to ~1.67 V followed by a voltage plateau region at ~1.7 V. The first-charge capacity value is 213 mAh g^{-1} (1.5 mol of Li). The difference between the discharge and charge capacities, which is the irreversible capacity loss during the first cycle, corresponds to 40%.

The second discharge profile is different from the first one indicating a different mechanism in operation. The discharge potential plateau was recorded at ~1.6 V. A good reversibility was observed for the subsequent cycles. Note that the electrochemical behaviour under a galvanostatic cycling matches well with the CV studies (Fig. 5).

In order to examine the electrochemical reactivity and stability of $Ni_{0.5}TiOPO_4$/C composite, 50 charge/discharge cycles were carried out at low rate. Fig. 6 shows the charge/discharge capacities of the Li//$Ni_{0.5}TiOPO_4$/C cell cycled between 0.9 V and 3 V at a low C rate of 0.05C. The first discharge capacity was 355 mAh g^{-1}. On charge, the capacity decreased to 213 mAh g^{-1}. Subsequent discharge and charge plot on top of each other, indicating stable capacity (~200 mAh g^{-1}) and high efficiency during the following cycles.

The cycle performance of Li//$Ni_{0.5}TiOPO_4$/C cells, cycled between 3.0 and 0.9 V vs. Li/Li^+, at different discharge rates are shown in Fig. 7. The 1st discharge capacity dropped with increasing current density (C-rate) from 209 mAh g^{-1} to 198 mAh g^{-1} and 195 mAh g^{-1} at C/10, C/5 and C/2, respectively. Good stability with high capacity retention of 95% up to 50 cycles was evidenced. For faster regime (1C rate), the capacity decreased continuously with cycling. The discharge capacity was 194 mAh g^{-1} in the 1st cycle but faded to 146 mAh g^{-1} after 50 cycles.

The rate capability of $Ni_{0.5}TiOPO_4$/C composite was investigated in the 0.9–3 V potential range at different C-rates from C/5 to 2C with an ascending order, followed by coming back to C/5 (Fig. 8). The cell was first discharged 5 times at C/5, the capacity decreases from 335 mAh g^{-1} (1st cycle) to 200 mAh g^{-1} (2nd cycle) and it becomes constant up to the 5th cycle. For other rates, the discharge capacity remains almost constant. At C/5 regime, the reversible capacity could still retain 198 mAh g^{-1}, illustrating higher discharge capacity and better cycle stability.

The $Ni_{0.5}TiOPO_4$/C composite presents excellent cycleability even at high rate. In comparison with the electrochemical properties of the pure $Ni_{0.5}TiOPO_4$ (Fig. 9), we could conclude that these good performances are related to the presence of carbon in $Ni_{0.5}TiOPO_4$/C composite. We are now attempting to use many carbon sources (glucose, PEG, etc.) with the aim to prepare a composite with sufficient and optimal carbon content.

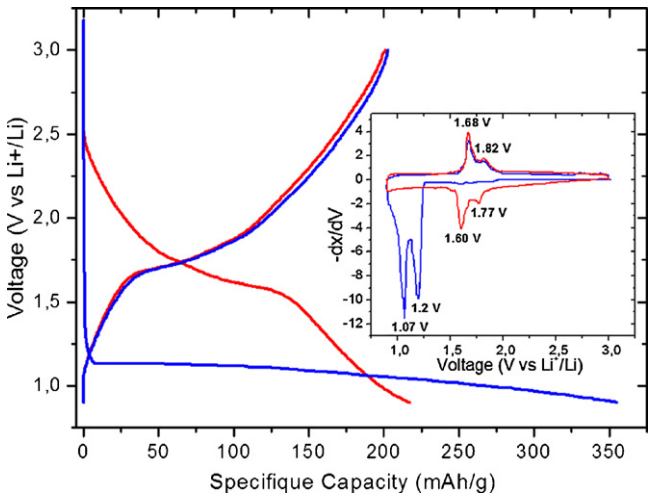

Fig. 5. First and second discharge/charge cycles of the Li//$Ni_{0.5}TiOPO_4$/C cell and their derivative curve. Voltage range: 0.9–3 V; rate: C/20.

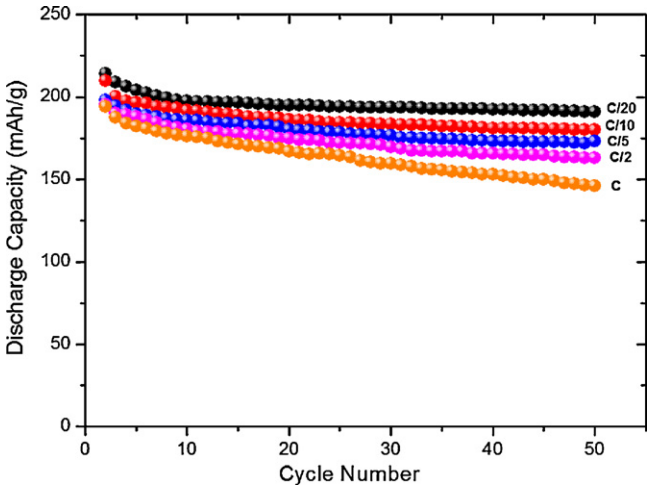

Fig. 7. Discharge specific capacity retention vs. cycle number for $Ni_{0.5}TiOPO_4$/C between 0.9 and 3 V at different rates.

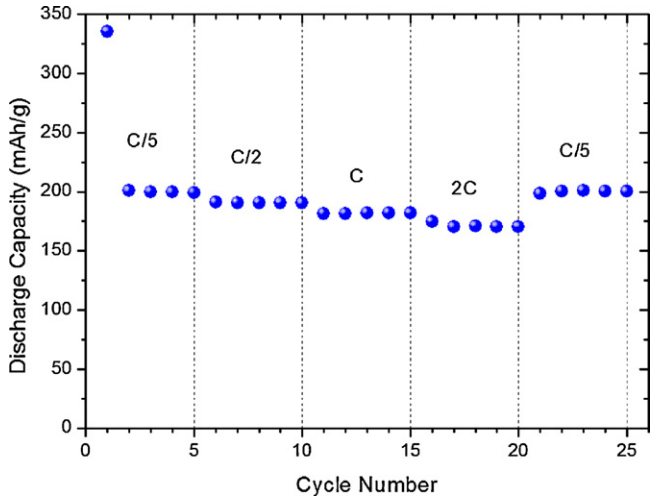

Fig. 8. Rate performances of the $Ni_{0.5}TiOPO_4$/C electrode at different rates.

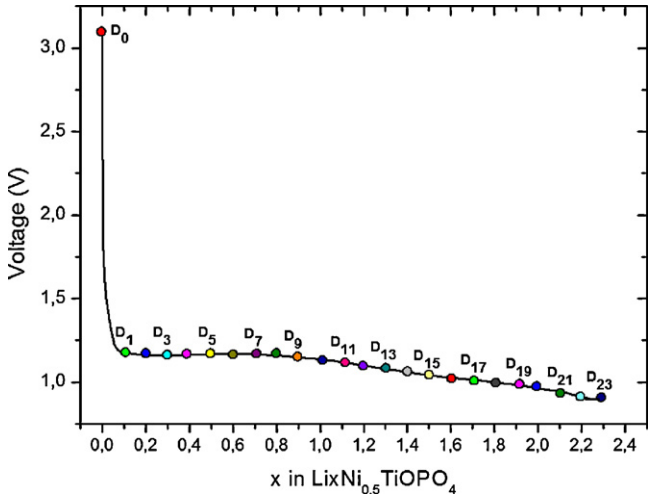

Fig. 10. First discharge curve of a Li//$Li_xNi_{0.5}TiOPO_4$/C cell at the C/5 rate from OCV to 0.9 V.

3.4. Structural changes

In order to understand the structural changes upon the 1st electrochemical lithium intercalation causing the high irreversible discharge capacity (Fig. 5), synchrotron-based *in situ* XRD technique was used. Fig. 10 shows the first discharge curve of Li//$Li_xNi_{0.5}TiOPO_4$/C cell using a constant current at a C/5 rate (5 h to intercalate 1 lithium ion). The reported D_i points in this figure correspond to the compositions analyzed by the *in situ* synchrotron XRD.

Fig. 11a shows the synchrotron diffraction of the fresh battery cell. Rietveld refinement confirmed that the pristine $Ni_{0.5}TiOPO_4$/C crystallizes in the monoclinic system with $P2_1/c$ space group. Additional diffraction peaks are attributed to the Li anode and polymer. Fig. 11b displays the *in situ* diffraction pattern of $Li_xNi_{0.5}TiOPO_4$/C collected at the end of the first discharge. The comparison between these two patterns clearly shows an important evolution of the structural features: the diffraction peaks broadened and a new phase appeared during the lithium insertion.

During the first discharge, 24 XRD scans were continuously collected, as indicated in Fig. 10, but only 13 XRD patterns are plot-

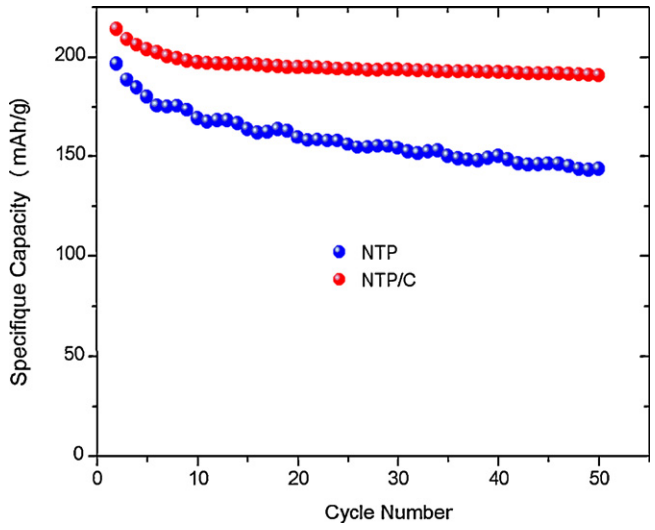

Fig. 9. Effect of the carbon coating on the electrochemical cycling of the $Ni_{0.5}TiOPO_4$. For more clarity, the comparison was done from the 2nd to the 50th discharge. Voltage range: 0.9–3 V; rate: C/20.

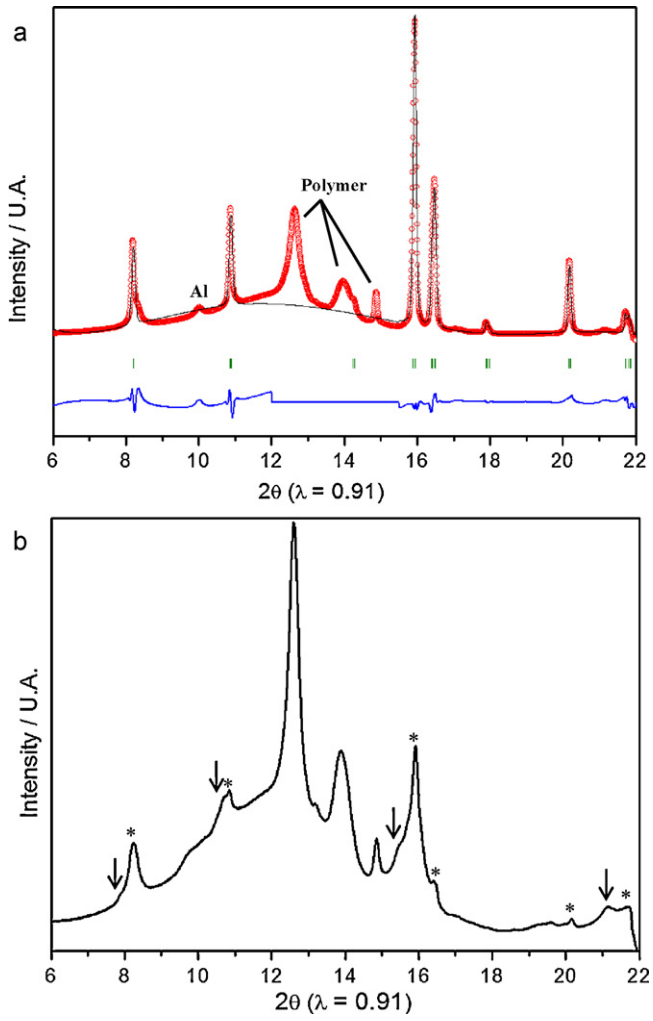

Fig. 11. Synchrotron diffraction patterns of (a) the fresh battery cell, and (b) at the end of the first discharge. The phase diffraction peaks are marked by "*" and the new phase diffraction peaks are marked by ↓.

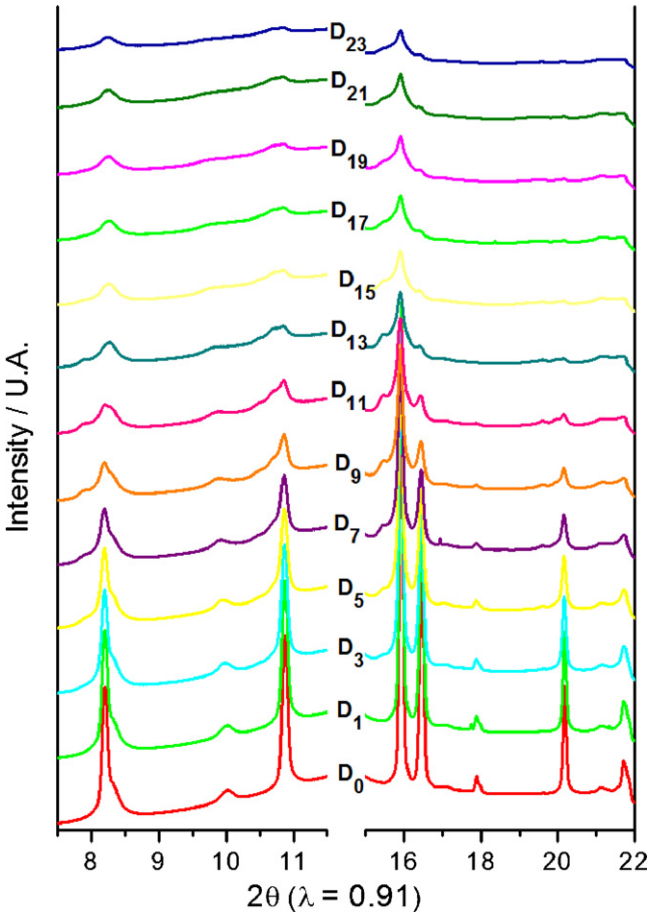

Fig. 12. *In situ* X-ray diffraction patterns of a Li//$Li_xNi_{0.5}TiOPO_4$/C cell discharged from 0.9 to 3 V at C/5 rate.

ted in Fig. 11 with the corresponding scan number indicated in the discharge curve. Two selected 2θ regions, $7.5^\circ < 2\theta < 11.5^\circ$ and $15^\circ < 2\theta < 22^\circ$, are displayed to show the structural evolution.

As can be seen from Fig. 12, no considerable structural change until scan D_5 was detected. From D_7 to D_{13}, a continuous decrease in the intensity of the peaks and the broad shoulders to the left of parent peaks are evidenced. This clearly indicates the presence a new phase accompanied by an amorphization of the starting material. After D_{13}, it was observed that both of the diffraction peaks of parent phase and those of the newly formed phase became broader and broader with lithium intercalation. This suggests the formation of defects (e.g. microstrain and stacking faults) within the material structure lattice or/and that the crystal particles cracked into smaller ones during the electrochemical process. Furthermore, even though the peak intensities of the parent phase considerably decreased with lithium intercalation, they did not disappear completely after the first discharge (Fig. 11b).

We have tried to refine the diffraction pattern collected after the first discharge (Fig. 11b) using monoclinic or orthorhombic structural models for the new phase. But none of them gave a satisfactory result. In fact, the very low crystallinity of the lithiated product coupled to the very weak intensities of the XRD peaks corresponding to the new phase lead to too little information to give any solid suggestions for structure or reaction mechanism during the first discharge process. At present, we will not concentrate on this challenge but continue to investigate how the structure changed during the first and the second discharge.

Fig. 13 displays the diffraction patterns of the Li//$Li_xNi_{0.5}TiOPO_4$/C cell after the 1st discharge/charge and

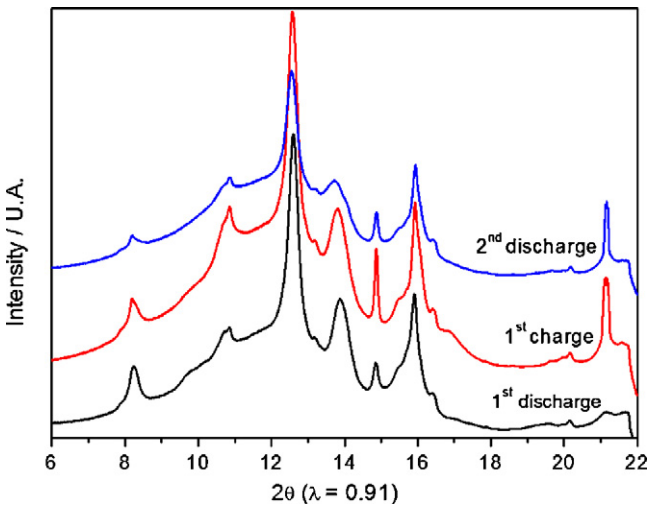

Fig. 13. *In situ* X-ray diffraction patterns of a Li//$Li_xNi_{0.5}TiOPO_4$/C cell recorded at the end of the 1st discharge; 1st charge and 2nd charge at a C/5 rate.

2nd discharge. The intensities of the diffraction peaks belonging to parent phase and new phase remains unchanged with cycling. Meanwhile, the peak formed at $2\theta \approx 21.15^\circ$ which disappears during the first discharge, remains unchanged for the subsequent charge–discharge. This peak, presumably from Li, comes from the lithium foil present as anode in the *in situ* battery.

Thus, the crystal structure of the studied phases is still complicated and needs to be completed by other sensitive techniques such as Li NMR, neutron diffraction, soft X-ray absorption spectroscopy (XAS). Indeed, we recently started the investigation of the $Li_xNi_{0.5}TiOPO_4$ phases (obtained chemically and electrochemically) by XAS, neutron diffraction and Squid measurements in order to present a general overview and the appropriate mechanism of the lithium insertion in this electrode material.

4. Conclusions

$Ni_{0.5}TiOPO_4$ phosphate exhibits a 3D framework built up from [PO_4] tetrahedra and [TiO_6] octahedra linked together by corners and form infinite chains along the *c*-axis. Nickel ions are located in the octahedral site sharing two faces with two [TiO_6] octahedra. The structural positions of transition metal ions explain the very low electronic conductivity of the studied compound. Thus, $Ni_{0.5}TiOPO_4$/carbon composite was prepared by using the sucrose as the carbon source. No structural differences with the pure $Ni_{0.5}TiOPO_4$ were evidenced. The use of this composite as active material in lithium batteries shows many properties: (i) an apparent improvement of the electrochemical performances in terms of discharge capacity, cycleability and rate capability; (ii) an irreversible capacity (around 40%) during the first discharge.

Thus, *in situ* synchrotron XRD study was used during the first discharge–charge cycle. The recorded patterns clearly show an irreversible peak broadening during the first discharge accompanied by the apparition of a new phase which remains stable during the subsequent cycles.

Acknowledgements

The authors gratefully acknowledge the financial support of the Swedish Research Council (VRMENA program), the Swedish Energy Agency and the Swedish Hybrid Vehicle Centre. Mrs. Maher Kenza would like to thanks the CNRST and the MENESFCRS Ministry for the scholarship.

References

[1] J.M. Tarascon, M. Armand, Nature (London) 404 (2001) 359.
[2] T. Nagaura, K. Tozawa, Prog. Batt. Sol. Cells 9 (1990) 209.
[3] O. Mao, R.A. Dunlap, J.R. Dahn, J. Electrochem. Soc. 146 (1999) 405.
[4] K.D. Kepler, J.T. Vaughey, M.M. Thackeray, Electrochem. Solid State Lett. 2 (1999) 307.
[5] Y. Idota, T. Kubota, A. Matsufuji, Y. Maekawa, T. Miyasaka, Science 276 (1997) 1395.
[6] I.A. Courtney, J.R. Dahn, J. Electrochem. Soc. 144 (1997) 2045.
[7] J. Chouvin, C. Branci, J. Sarradin, J. Olivier-Fourcade, J.C. Jumas, B. Simon, P. Biensan, J. Power Sources 81–82 (1999) 277.
[8] H. Huang, E.M. Kelder, L. Chen, J. Schoonman, J. Power Sources 81–82 (1999) 362.
[9] P. Poizot, S. Laruelle, S. Grugeon, L. Dupont, J.-M. Tarascon, Nature 407 (2000) 496.
[10] P. Poizot, S. Laruelle, S. Grugeon, L. Dupont, J.-M. Tarascon, J. Power Sources 97–98 (2001) 235.
[11] F. Badway, I. Plitz, S. Grugeon, S. Laruelle, M. Dolle, A.S. Gozdz, J.-M. Tarascon, Electrochem. Solid State Lett. 5 (2002) A115.
[12] E. Baudrin, S. Laruelle, S. Denis, M. Touboul, J.-M. Tarascon, Solid State Ionics 123 (1999) 139.
[13] K.M. Colbow, J.R. Dahn, R.R. Haering, J. Power Sources 26 (1989) 397.
[14] I. Belharouak, K. Amine, Electrochem. Commun. 7 (2005) 648.
[15] K. Maher, K. Edström, I. Saadoune, T. Gustafsson, M. Mansori, Electrochim. Acta 54 (2009) 5531.
[16] P. Gravereau, J.P. Chaminade, B. Manoun, S. Krimi, A. El Jazouli, Powder Diffr. 14 (1999) 10.
[17] J. Rodriguez-Carvajal, Fullprof Program for Rietveld Refinement, version 3.7, LLB JRC, 1997.
[18] T. Gustafsson, J.O. Thomas, R. Koksbang, G.C. Farrington, Electrochim. Acta 37 (1992) 1639.
[19] A.S. Prakash, P. Manikandan, K. Ramesha, M. Sathiya, J.-M. Tarascon, A.K. Shukla, Chem. Mater. 22 (2010) 2857.
[20] K. Ariyoshi, T. Ohzuku, J. Power Sources 174 (2007) 1258.
[21] A.N. Jansen, A.J. Kahaian, K.D. Kepler, P.A. Nelson, K. Amine, D.W. Dees, D.R. Vissers, M.M. Thackeray, J. Power Sources 81–82 (1999) 902.